Simulation of transient energy distributions in sub-ns streamer formation

C S MacLachlan, H E Potts and D A Diver

SUPA, School of Physics and Astronomy, Kelvin Building, University of Glasgow, Glasgow G12 8QQ, UK

Abstract. Breakdown and streamer formation is simulated in atmospheric pressure nitrogen for a 2-D planar electrode system. A PIC code with multigrid potential solver is used to simulate the evolution of the non-equilibrium ionization front on sub-nanosecond timescales. The ion and electron energy distributions are computed, accounting for including inelastic scattering of electrons, and collisionally excited metastable production and ionization. Of particular interest is the increased production of metastable and low-energy ions and electrons when the applied field is reversed during the progress of the ionization front, giving insight into the improved species yields in nanosecond pulsed systems.

PACS numbers: 52.77.Fv, 52.20.-j,52.65.-y, 51.15.+v, 52.25Jm

Submitted to: *Plasma Sources Sci. Technol.*

1. Introduction

Many conventional plasma devices, such as those used in industrial processes, have discharge lifetimes much longer than any intrinsic plasma timescale. When this is the case the plasma has time to relax into an equilibrium (albeit driven). For these plasmas the initiation of the discharge, on breakdown timescales of tens of nanoseconds [1], is a unimportant fraction of the plasma's lifetime. However, there are some devices (such as microdischarge plasma devices, and pulsed-power sources) which evolve on timescales where the breakdown process is significant compared with the plasma duration. In these early stages, the plasma is far from equilibrium, and its evolution can be dominated by complicated, transient charge structures. Such devices can exploit non-equilibrium processes [2, 3], and plasma diagnostics are evolving to the extent that sub-nanosecond evolution is now possible to measure [4].

For example, applying a 20ns pulse to a DC microdischarge produces an increase in the observed emission from excimer molecules [5], due to the higher electron number density and mean energy resulting from the pulse compared with the purely DC case. The use of short-pulse systems has become widespread, being used in a variety of commercial devices: decomposition of harmful gases, ozone generation [6], treatment of algae bloom, concrete recycling [7] and microbial decontamination [8]. The rise time and pulse width in these systems can be on the order of nanoseconds, and pulsing the discharge reduces the field strength required to breakdown the gas [9]. Charged particles and metastable states remain in the gas between pulses; this residue makes subsequent breakdowns easier.

It has been found that nanosecond pulses of MVm^{-1} electric fields can be used in cell treatment [10]. The electric field can cause programmed cell death without permanently damaging the outer cell membrane. Manipulation of cellular structures requires pulses short enough to bypass the membrane and deposit the energy inside.

This has led to a renewed interest in the first few nanoseconds of plasma initiation, and not just in application physics: atmospheric studies of transients such as sprites [11, 12] are now beginning to yield important insights into naturally occurring particle acceleration.

When sub-microsecond pulses are used, the initiation of the plasma becomes a significant factor in its evolution; understanding the breakdown of the neutral gas, the population of excited species and the (non-equilibrium) transient electron energy distribution function are key to controlling and characterising these short pulse plasmas, and are addressed by the simulations presented in this paper.

2. Description of physical setup

The particle model described in [13] is used to model an electron avalanche in molecular Nitrogen gas at atmospheric pressure. A simple parallel plate device is modelled; the computational domain addresses a 1mm gap, across which an electric field of $12\mathrm{MVm}^{-1}$

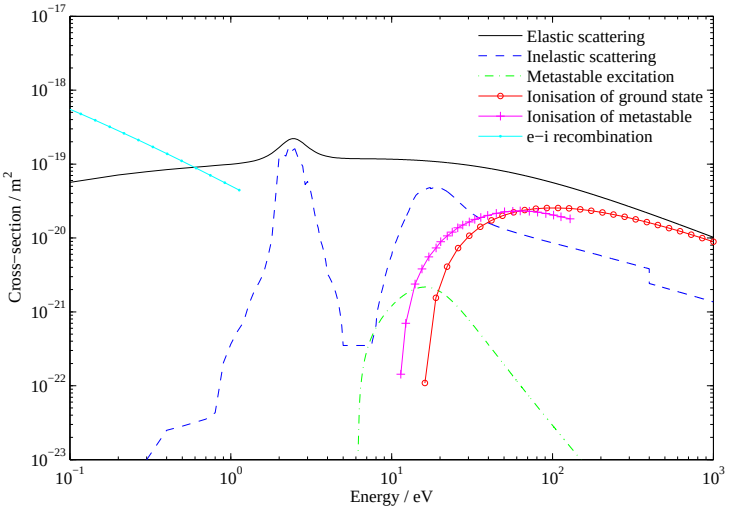

Figure 1. Cross-sections for molecular Nitrogen.

is applied. The avalanche is initiated from a single electron-ion pair at rest, situated near the cathode. The simulation is confined to the plane, to simplify the computational effort.

In the first simulation the electron avalanche evolves in an applied DC electric field. In the second case, the direction of the electric field is reversed after 1ns, in order to explore resultant enhanced production of metastable states in a rapidly oscillating electric field. The aim is to maximise the number of metastables without inducing full breakdown and the associated current spike across the device.

The particle model will be used to calculate the trajectories of the electrons, positive ions and one metastable species (N_2 $A^3\Sigma_u^+$). An isothermal background of neutrals consistent with molecular Nitrogen at atmospheric pressure and a temperature of approximately room temperature (300K) is assumed.

The following collisions are included: elastic scattering [14], inelastic scattering [14, 15], metastable excitation ($A^3\Sigma_u^+$) [14], ionisation [14], metastable ionisation [16] and electron-ion recombination [14]. Figure 1 shows the energy dependence of the cross-sections. The ionisation energy threshold of N_2 is 15.58 eV, the excitation threshold for the metastable is 6.17eV and the energy threshold for ionisation of the $A^3\Sigma_u^+$ metastable is 11.4 eV.

3. Initial conditions for the simulation

The simulation is carried out in a two-dimensional computational domain comprising 1025×513 grid cells, with uniformity assumed in the third dimension (or at least that the scale length for variation in the third direction is very much larger than any scale length in the plane). A multi-grid method [17, 18, 19] is used to greatly improve the accuracy of the potential solver. The multi-grid method is not the same as adaptive

grid refinement techniques in which the computational mesh comprises areas of different spatial resolution [20]. Instead, multi-grid iteration ensures that the numerical solution converges efficiently and accurately, taking account of the influence of distant solution features that would otherwise take several iterations (under the usual finite-difference 'nearest-neighbour' interaction) to exert the correct local influence.

If a particle collides with a boundary then it is deleted. The maximum number of particles that can be stored during the simulation is 17.5 million per type.

The potential at electrode left (x=1) and right (x=N_x) boundaries are fixed at −6kV and +6kV respectively. The non-electrode boundaries are assumed to be far from the computational boundary and so, zero-value von Neumann boundaries are used, equivalent to setting the distant electric field to zero.

In the DC case the electron-ion pair starts the position (15, $N_y/2$, $N_z/2$) and in the case where the field is reversed ($N_x/3$, $N_y/2$, $N_z/2$). The position of the electron is changed in the field reversal case to ensure the avalanche does not encounter the $x = 1$ boundary too early after the field is reversed.

4. Simulation results

4.1. General observations

Each of the following results exhibit similar physical features. When describing the electron avalanches, the ionisation front of electrons will be referred to as the 'head' and the trail of ions is termed the 'tail'.

There are common observations relevant to all simulation results here. Collisional and electrostatic effects influence the spatial distribution of the avalanche: in the early stages the diffusion of the avalanche is dominated by the effect of elastic collisions, but as the number of electrons grows the diffusion is enhanced by their mutual repulsion.

There is also evidence of instabilities in the electron head. Bifurcation of the avalanche can be seen, resulting from an irrecoverable perturbation in the self-field as the streamer shows the onset of branching [21, 20, 22]. Ionisation occurs at the edges of the field perturbations and increases the size of the instability region.

4.2. DC electric field

This is the simple planar case of an electron-ion pair accelerating in the electric field created by two planar electrodes held at opposing potentials (±6kV). The spatial evolution of the electron avalanche is shown in figure 2. Snapshots of the electron density, ion density, metastable density and the total electric potential are shown for a selection of times, with the electron and ion energy distribution functions for the same time selections shown in figure 3.

It is clear that the self-field of the electron head becomes important at around 1ns into the evolution, at which point the potential across the gap is clearly distorted; at

1.2ns, the familiar concentration of electron density in an arc at the head has developed, and enhanced lateral diffusion is evident.

At 1.4ns, the electron head begins to filament as a result of Laplacian instability [23, 24], shown more clearly in the shape of the distorted potential plot; this becomes more pronounced as the avalanche continues to evolve, and the electron numbers increase. The net metastable density production begins to slow from this point onwards, due the rising level of metastable ionization produced by the growing population of electrons having energies in excess of 11eV. Also, the depletion of electron population at energies of around 2-3eV becomes marked here, as the inelastic cross-section reaches a maximum.

4.3. Field reversal

The simple case in the previous section is now extended to cover the situation in which the polarity of the planar electrodes is 'instantaneously' reversed, in order to describe what happens when a developing avalanche encounters a radically different electrical environment. Figure 4 shows the spatial evolution of the electron avalanche when the electric field is reversed; note that this is a 'perfect' reversal, in that there are no electric field transients associated with the technical process of the field reversal itself. In this model calculation the reversal occurs during a single timestep, rather than gradually: the motivation is to show how the electron dynamics is modified by the pre-existing, comparatively static ion tail, leading for example to enhanced metastable creation. Although the calculation is therefore not entirely self-consistent, it can still be informative, particularly in the case where there is a a discontinuous, sudden change in the local electrical environment (arising for example from an external field-creating event, such as a cosmic ray strike [25, 26]).

Snapshots of the electron density, ion density, metastable density and the total electric potential are shown for an illustrative selection of times.

After the field reversal the particle densities shown in figure 4 have a distinctive dumbbell shape. As the electron avalanche forms in the forward field direction the typical avalanche shape forms. When the field direction reverses the lower energy electrons in the middle and tail are accelerated in the new field direction and reach ionisation energies before the high energy electrons in the avalanche head. The electrons in the tail effectively form a new avalanche and the typical tadpole shape is produced again, this time pointing in the opposite direction. The electron and ion energy distribution functions for the same time selections are shown in figure 5.

4.4. Comparing DC and reversed electric fields

The spatial distribution of the particles in the two cases is different because the fields point in opposite directions during the later stages of the avalanche.

The electron energy distribution functions in both the DC and field reversal cases have quite complicated shapes. Figure 6 shows the eedfs at time 1.60ns with the cross-

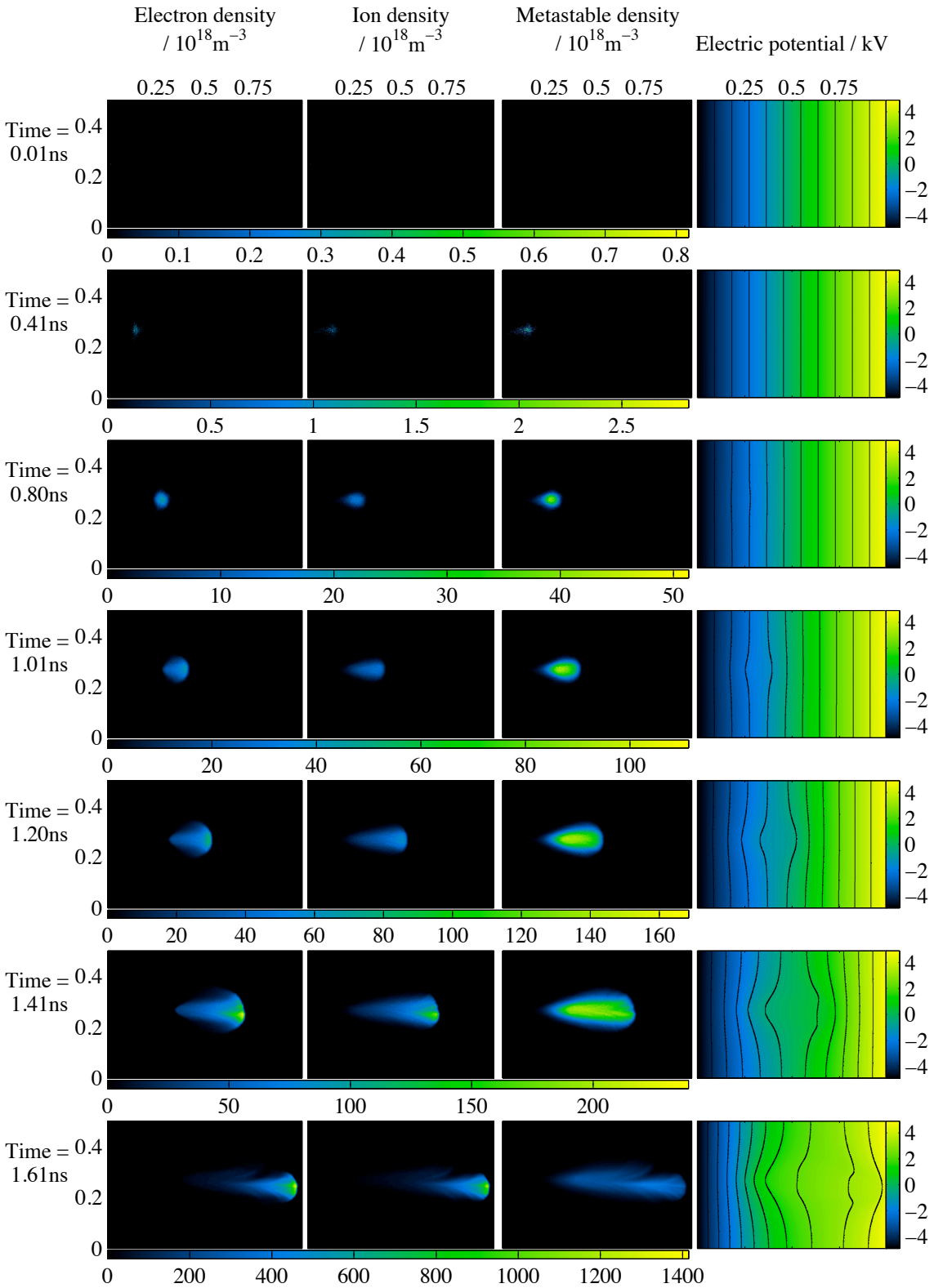

Figure 2. Evolution of the electron avalanche in a 1mm gap of atmospheric pressure Nitrogen with an electric field of 12MVm^{-1}. The colour scale for the density plots changes for each series of snapshots. The numerical range of the density scale is shown beneath the density plots. The colour scale for the electric potential is situated to the right of each plot. The x- and y-axes on each plot give the spatial variation in the x and y directions and are expressed in units of mm.

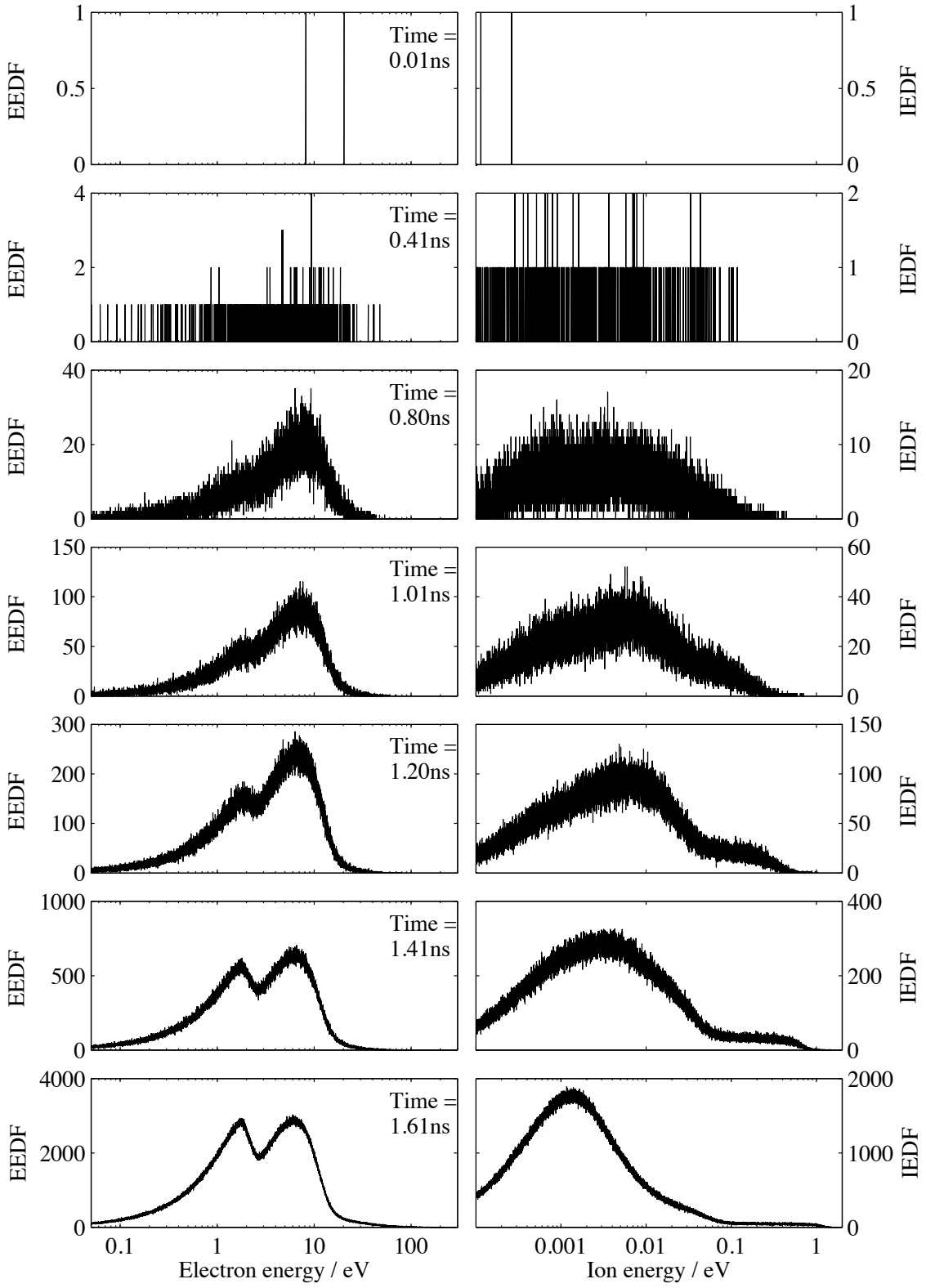

Figure 3. Evolution of the electron and ion energy distribution functions in a DC electric field.

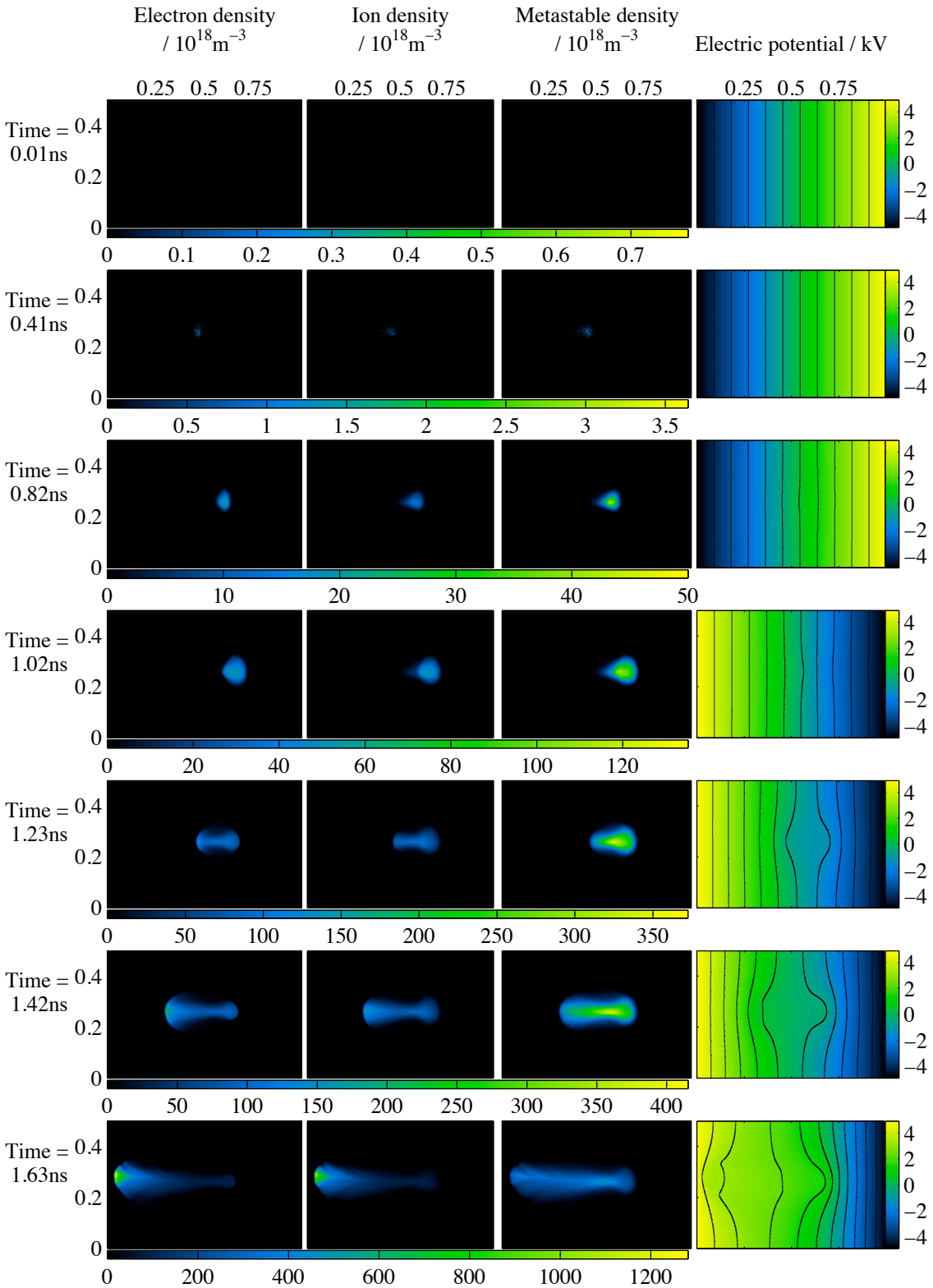

Figure 4. Evolution of the electron avalanche in a 1mm gap of atmospheric pressure Nitrogen with an electric field of 12MVm^{-1} reversed at 1ns. The colour scale for the density plots changes for each series of snapshots. The numerical range of the density scale is shown beneath the density plots. The colour scale for the electric potential is situated to the right of each plot. The x- and y-axes on each plot give the spatial variation in the x and y directions and are expressed in units of mm.

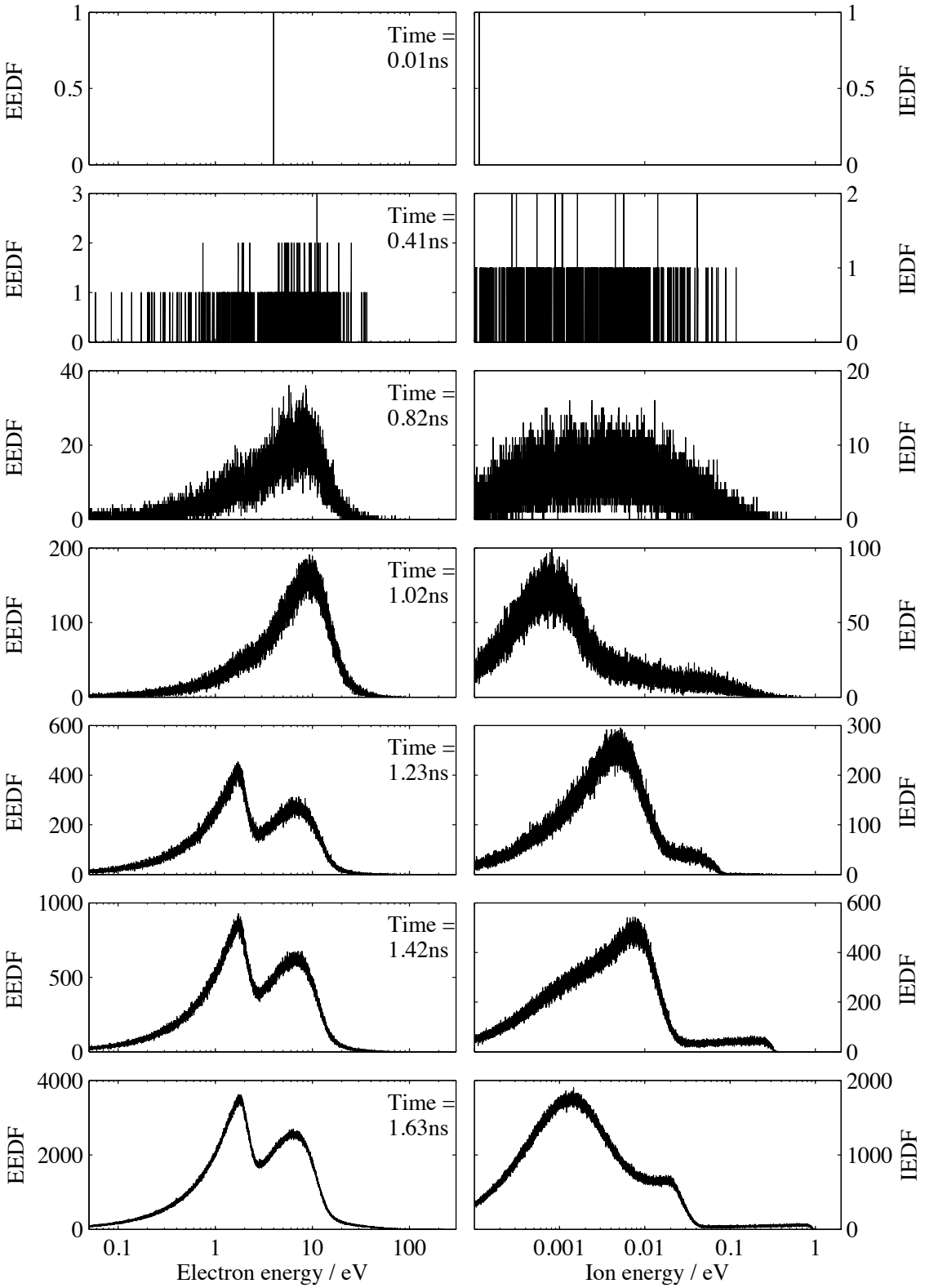

Figure 5. Evolution of the electron and ion energy distribution functions for the case in which the electric field is reversed after 1ns.

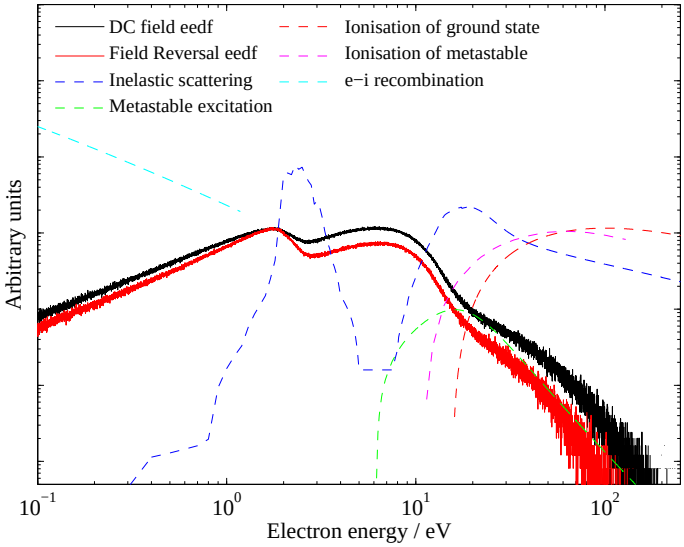

Figure 6. Plot showing the normalised energy distributions and the normalised cross-sections for the time $1.6 \times 10^{-9} s$. Only the cross-sections that result in an energy loss are shown.

sections of: inelastic scattering, metastable excitation, metastable ionisation, neutral ionisation and recombination superimposed. The inelastic reactions have a noticeable effect on the eedfs. At approximately 2eV there is a dip in the electron energy distribution, corresponding to the peak in the inelastic cross-section; above 10eV the rapid increase in metastable excitation, inelastic scattering and ionisation processes combine to strongly depress the EEDF.

The energy distributions show that the populations of both the electrons and ions at lower energies are greater when the field is reversed. This is expected since the direction of the field initially decelerates the charged particles.

Figure 7 compares the number of species created in the avalanche for both electric field cases. There is a clear increase in the number of all species just after the time when the field is reversed, and for the next ~ 0.5ns. The increase in the ionisation and metastable excitation rate is caused by the alignment of the self-field and the applied field. When the applied field is reversed it is in the same direction as the self-field created by the electron head and ion tail. This means that the value of the ambient electric field is higher than it would be when there is no field reversal, resulting in a boost both in the electron acceleration and in the particle production rate. As the avalanche reverses its bulk motion the particle production rate drops and, over time, the numbers of particles in the DC avalanche catch up with the field-reversed case, and in fact, exceed them. This is principally caused by an increase in the population of lower energy particles caused by the retardation caused by the field reversal, which in turn increases the number of recombination events and thereby depletes the plasma population over time.

In figure 8 the energy probability functions of the electrons and ions for each of the

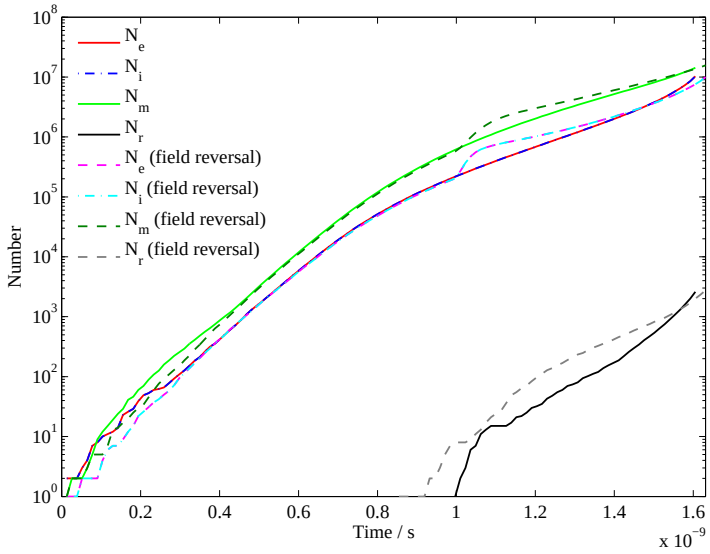

Figure 7. Comparison of the numbers of each species for DC and reversed electric fields. The legend entries: N_e, N_i, N_m, N_r correspond to the number of electrons, ions, metastables and the total number of neutrals formed from recombination reactions respectively. Note that the field reversal occurs at 1ns.

electric field cases are shown at 1.6ns, the final time point of the simulation. The plots show that none of the energy distributions can be described fully using Maxwellian or Druyvesteyn distributions: the former would be linear, and the latter parabolic on such a graph. Given that the electron plots are significantly distorted below approximately 20eV, it's clear that neither equilibrium description is adequate, so the electrons are yet to equilibrate. Note that the eepfs for the two electric field cases have similar shapes but there is a smaller number of particles in the field reversal case compared to the DC case: this can be seen by comparing the species numbers at the right-hand edge of figure 7. It is also notable that there are significantly fewer energetic ions for the field reversal case, consistent with the deceleration of positive ions as the field reverses.

5. Conclusions

A robust particle model has been implemented and used to model the early stages of electron avalanche development. The populations of electrons, ions and N_2 $A^3\Sigma_u^+$ metastables has been calculated, along with the total electric potential and the energy distribution of the electrons and ions. The results from the simulations highlight the non-equilibrium nature of the tenuous plasma on a nanosecond timescale, showing how the species evolve as a result of electron-moderated processes, reflecting the energy structure of the reaction cross-sections. The field-reversed calculations show the significance of the relatively static tail of positive ions when the electric field drives the electron front back over the pre-formed ionization trail. Significant enhancements of metastables and

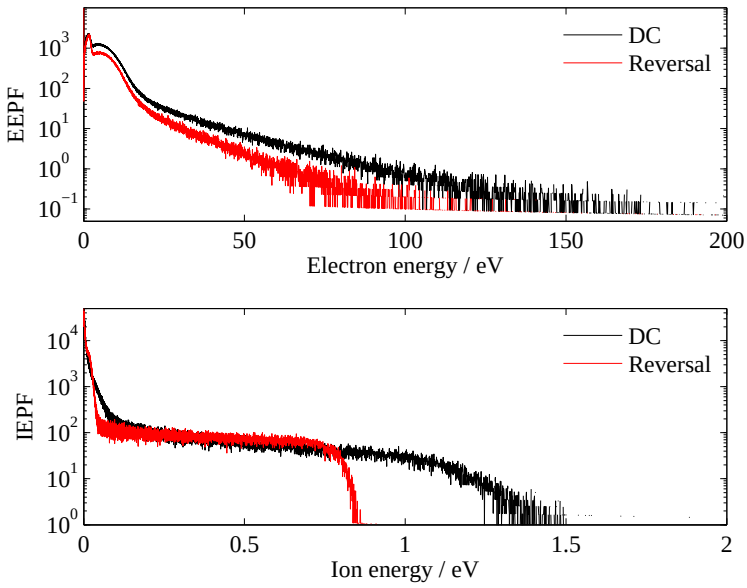

Figure 8. Comparison of the electron and ion energy probability functions for DC and reversed electric fields at time 1.61×10^{-9}s.

low-energy species results, consistent with the nanosecond pulsed-power experiments that show improved yields of reactants compared with steady-state conditions [27].

Many existing simulations of gas breakdown have been carried out with fluid models (for example, [28, 29, 30]) which require assumptions about the initial plasma density and its distribution [12]. In general, such models depend on the drift-diffusion assumption in which the electron distribution is taken to be fully relaxed, reflecting the fluid-nature of the analysis. The simulations presented here address directly the short time-scale evolution before that relaxed state is reached, and therefore do not (and cannot) exploit the drift-diffusion simplification. Instead, using only the imposed and self-generated electrical environment and an initial electron-ion pair, the development of the non-equilibrium avalanche is simulated, including the direct computation of the particle energy distributions. Hence the calculations presented here are the precursors to the relaxed distributions used in fluid calculations, and so offer a short time-scale complement to drift-diffusion approaches. There are avalanche PIC simulations [31] and hybrid fluid-PIC codes [32, 33], but the advantage of the simulation reported here is that by calculating the evolving distribution functions in detail, comprehensive and accurate transient diagnostic information can be computed, allowing detailed characterisation of the non-equilibrium plasma evolution. Short time-scale calculations are a valuable complementary technique to approaches such as BOLSIG [34], where non-equilibrium electron distribution functions are inferred from localised uniform electric field conditions, and used to correct transport and rate coefficients in the fluid limit.

The metastable population plays a key part in the breakdown voltage conditions

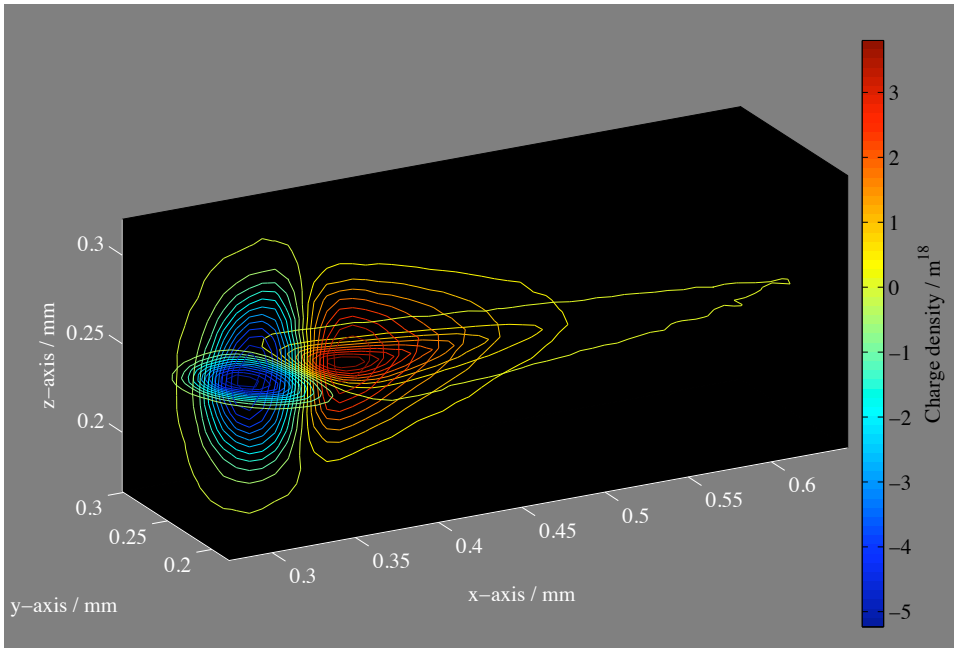

Figure 9. Three-dimensional contour plot of charge density showing typical structure of avalanche.

in pulsed plasmas [9], since they have a long lifetime compared to the pulse length: for example, the N_2 $A^3\Sigma_u^+$ metastable has a lifetime of $\sim$2.7s. Hence the metastables can be ionised by lower energy electrons than is required for a ground-state neutral, thus reducing the requirement for breakdown (the metastables act as energy stores, allowing a two-step processes to lead to ionization). This underlines the necessity for including the evolution of such species in any comprehensive simulation, along with the appropriate instantaneous and self-consistent electron energy distribution.

Finally, it is important to assess any implications from the two-dimensional nature of this calculation. It is generally true that a 2-D calculation over-estimates the electron density, since it assumes similar density above and below; this becomes particularly true at the avalanche leading edge. However, a full 3-D calculation is underway (and will be reported soon), removing such geometric effects. For comparison, the full electron head shape in 3-D is shown in figure 9.

6. Acknowledgements

CSM is grateful to EPSRC for studentship funding, and HEP acknowledges financial support from both SUPA and an EPSRC KTA award (EP/H500138/1). We are also happy to acknowledge continuing support from STFC grant ST/I001808/1.

References

[1] R C Fletcher 1949 *Phys. Rev.* **76** 1501–11

[2] J G Eden and S-J Park 2005 *Plasma Physics and Controlled Fusion* **47** B83–B92 .

[3] K H Becker, K H Schoenbach, and J G Eden 2006 *Journal of Physics D: Applied Physics* **39**R55–R70

[4] R. Brandenburg, T. Hoder, and H.-E. Wagner 2008 *Plasma Science, IEEE Transactions on* **36**1318 –19

[5] Mohamed Moselhy, Isfried Petzenhauser, Klaus Frank, and Karl H Schoenbach 2003 *Journal of Physics D: Applied Physics* **36** 2922-27

[6] X Duten, M Redolfi, N Aggadi, A Vega, and K Hassouni 2011 *Journal of Physics D Applied Physics* **44** 415202

[7] H Akiyama, S Sakai, T Sakugawa, and T Namihira 2007 *Dielectrics and Electrical Insulation, IEEE Transactions on* **14** 825–33

[8] J Ehlbeck, U Schnabel, M Polak, J Winter, T von Woedtke, R Brandenburg, T von dem Hagen and K-D Weltmann 2011 *Journal of Physics D Applied Physics* **44** 013002

[9] T Shao, G Sun, P Yan, and S Zhang 2007 *Dielectrics and Electrical Insulation, IEEE Transactions on*, **14** 813–19

[10] P Krishnaswamy, A Kuthi, P T Vernier and M A Gundersen 2007 *Dielectrics and Electrical Insulation, IEEE Transactions on* **14** 873–77

[11] M Fullekrug 2006 *American Journal of Physics* **74** 804–05

[12] A Luque and U Ebert 2012 *Journal of Computational Physics* **231** 904–18

[13] C S MacLachlan, D A Diver and H E Potts 2009 *New Journal of Physics* **11** 063001

[14] T Tabata, T Shirai, M Sataka and H Kubo 2006 *Atomic Data and Nuclear Data Tables* **92** 375–406

[15] A V Phelps and L C Pitchford 1985 *Physical Review A* **31** 2932–49

[16] D Ton-That and M R Flannery 1977 *Physical Review A* **15** 517–26

[17] U Trottenberg, C W Oosterlee, and A Schüller *Multigrid*. Elsevier Academic Press, 2001.

[18] W L Briggs, V E Henson, and S F McCormick. *A multigrid tutorial (2nd ed.)*. Society for Industrial and Applied Mathematics, Philadelphia, PA, USA, 2000.

[19] C S MacLachlan 2009 *Numerical modelling of low temperature plasma*. PhD thesis, School of Physics and Astronomy, University of Glasgow, Glasgow G12 8QQ

[20] C Montijn, W Hundsdorfer and U Ebert 2006 *Journal of Computational Physics* **219** 801–35

[21] S Pancheshnyi, M Nudnova and A Starikovskii 2005 *Phys. Rev. E* **71** 016407

[22] Manuel Arrayás, Marco A Fontelos and José L Trueba 2005 *Phys. Rev. Lett.* **95** 165001

[23] G Derks, U Ebert and B Meulenbroek 2008 *Journal of NonLinear Science* **18** 551–90

[24] M Arrayás, S Betelú, M Fontelos, and J Trueba 2008 *SIAM Journal on Applied Mathematics*, **68** 1122–1145

[25] M Füllekrug, R Roussel-Dupré, E M D Symbalisty, O Chanrion, A Odzimek, O van der Velde and T Neubert 2010 *Journal of Geophysical Research (Space Physics)* **115** A00E09

[26] A V Gurevich, G G Mitko, V P Antonova, A P Chubenko, A N Karashtin, S V Kryukov, A S Naumov, L V Pavljuchenko, M O Ptitsyn, V A Ryabov, S Y Shalamova, A L Shepetov, Y V Shlyugaev, L I Vildanova and K P Zybin 2009 *Physics Letters A* **373** 3550–53

[27] T Matsumoto, D Wang, T Namihira, and H Akiyama 2011 *Japanese Journal of Applied Physics* **50** 080000

[28] P A Vitello, B M Penetrante and J N Bardsley 1994 *Phys. Rev. E* **49** 5574–98

[29] S K Dhali and P F Williams 1987 *Journal of Applied Physics* **62** 4696–707

[30] M Arrayás, U Ebert and W Hundsdorfer 2002 *Phys. Rev. Lett.* **88** 174502

[31] B J P Dowds, R K Barrett, and D A Diver 2003 *Physical Review E* **68** 026412

[32] Chao Li, U Ebert, and W Brok 2008 *Plasma Science, IEEE Transactions on* **36** 910–11

[33] W J M Brok, E Wagenaars, J van Dijk and J J A M van der Mullen 2007 *IEEE Transactions on Plasma Science* **35** 1325–34

[34] G J M Hagelaar and L C Pitchford 2005 *Plasma Sources Sci. Technol.* **14** 722-33